JOURNAL OF GEOPHYSICAL RESEARCH, VOL. 114, A12201, doi:10.1029/2009JA014530, 2009

Temporal evolution of proton precipitation associated with the plasmaspheric plume

M. Spasojevic[1,2] and S. A. Fuselier[1]

Received 3 June 2009; revised 10 August 2009; accepted 19 August 2009; published 1 December 2009.

[1] The temporal evolution of afternoon sector proton precipitation observed by a global auroral imager is examined in detail for two case events. We focus on precipitation regions that are magnetically mapped to the plasmapause and plasmaspheric plume regions. The spatial and temporal variation of the plume-associated precipitation, including its relationship to the main proton oval, is dependent on the prevailing solar wind and magnetospheric driving conditions. Two contrasting events are presented here in association with 1) a substorm injection and 2) a northward IMF turning. We find that proton precipitation within the plasmaspheric plume is a persistent feature during geomagnetically disturbed periods, but the precipitation regions only appear latitudinally detached from the main proton oval under specific conditions. The evolution in both time and space of the plume-associated precipitation regions is consistent with theoretical predictions for EMIC wave scattering of protons in the ring current energy range.

Citation: Spasojevic, M., and S. A. Fuselier (2009), Temporal evolution of proton precipitation associated with the plasmaspheric plume, *J. Geophys. Res.*, *114*, A12201, doi:10.1029/2009JA014530.

1. Introduction

[2] Cyclotron resonant wave-particle interactions provide an efficient means of transferring energy and momentum within the Earth's magnetosphere. One wave mode of particular interest is electromagnetic ion cyclotron (EMIC) waves [*Anderson et al.*, 1992a, 1992b; *Fraser et al.*, 1992, 1996; *Bräysy et al.*, 1998; *Erlandson and Ukhorskiy*, 2001; *Fraser and Nguyen*, 2001]. These intense (1–10 nT) plasma waves are generated by the ring current proton temperature anisotropy ($T_\perp > T_\parallel$) in spectral bands below the local ion gyrofrequencies. The generation and growth of EMIC waves can result in pitch angle diffusion of the source protons into the loss cone. In addition, parasitic wave-particle interactions can modify other particle distributions. For example, EMIC waves can heat heavy ion populations including ring current O^+ ions (>1 keV) [*Thorne and Horne*, 1993, 1994] and suprathermal He^+ ions (10's to 100's of eV) [*Horne and Thorne*, 1997]. The waves may also play a role in heating thermal electrons in the outer plasmasphere leading to the formation stable auroral red arcs in the ionosphere [*Cornwall et al.*, 1971; *Thorne and Horne*, 1992; *Gurgiolo et al.*, 2005]. Also, through anomalous resonance, EMIC waves can interact with relativistic electrons resulting in losses at energies >1–2 MeV [*Thorne and Kennel*, 1971; *Lyons and Thorne*, 1972; *Meredith et al.*, 2003; *Millan et al.*, 2002], and such interactions may contribute significantly to pitch angle scattering and relativistic electron depletion during the main phase of large geomagnetic storms [*Bortnik et al.*, 2006; *Jordanova et al.*, 2008].

[3] Statistically, EMIC waves are most frequently observed in the outer dayside magnetosphere in association with highly anisotropic proton distributions resulting from solar wind compression of the dayside magnetic field [*Anderson et al.*, 1992a; *Anderson and Hamilton*, 1993]. Within the inner magnetosphere, the waves occur most frequently and are the most intense during geomagnetic storms [*Bräysy et al.*, 1998; *Erlandson and Ukhorskiy*, 2001] and in regions of enhanced cold plasma density such as the plasmaspheric plume [*Fraser and Nguyen*, 2001]. The waves are preferentially generated within the plume since the presence of cold plasma reduces resonant proton energy into the ring current energy range (10's to a few 100 keV) where fluxes are higher and thus more protons are available for resonance [*Kennel and Petschek*, 1966]. In addition, the plasmapause gradient or filamentary density structures within the plume [*Spasojević et al.*, 2003; *Goldstein et al.*, 2004] can act to guide waves along the field line leading to enhanced convective growth rates [*Thorne and Horne*, 1997].

[4] The distribution of EMIC waves during disturbed intervals and resultant proton precipitation has been extensively studied using global kinetic simulations of the ring current [e.g., *Jordanova et al.*, 2007; *Khazanov et al.*, 2007, and references therein]. However, observational verification of the predicted global wave patterns is inherently difficult since the waves are spatially and temporally localized and spacecraft coverage is limited. Empirical wave models can provide a basis for comparison, but coarse binning of geomagnetic conditions leads to the smearing of spatial and temporal effects such that differences between individual events are unlikely to be captured.

[1]Lockheed Martin Advanced Technology Center, Palo Alto, California, USA.
[2]Also at Space, Telecommunications and Radioscience Laboratory, Stanford University, Stanford, California, USA.

0148-0227/09/2009JA014530$09.00

[5] On the other hand, there is increasingly clear evidence linking EMIC waves with ring current proton pitch angle scattering. From observations in the equatorial plane, *Erlandson and Ukhorskiy* [2001] reported simultaneous occurrence of EMIC waves and enhanced fluxes of protons in the loss cone. Precipitating protons are more easily observed at low altitudes (as a result of the increased loss cone angle). As a result, several studies have reported a strong correlation between low-altitude proton precipitation equatorward of the isotropic boundary (the sharp boundary that exists at all local times and separates the poleward zone of energetic particle precipitation that is isotropic across the loss cone from the equatorward zone of weak loss cone filling [e.g., *Sergeev et al.*, 1997]) and ground-based measurements of waves in the Pc1 frequency range (0.1–2 Hz) including narrowband Pc1 pulsations and Intervals of Pulsation of Diminishing Period (IPDP) [*Søraas et al.*, 1980; *Yahnina et al.*, 2000, 2002, 2003]. Both of these pulsations are ground-based signatures of EMIC waves [*Kangas et al.*, 1998]. The close relationship between the waves and the precipitation throughout the large data sets examined led *Yahnina et al.* [2003, p. 2282] to remark that "the localized proton precipitation marks the Pc1 source field lines."

[6] In studies of ground-based EMIC observations, *Engebretson et al.* [2008] confirmed past reports that the waves are most often observed during late recovery phase of magnetic storms. The absence of waves in ground-based recordings during the onset and main phase of storms has previously been attributed to a lack of propagation to the ground. However, in correlating wave observations to low altitude satellite observations of precipitating protons in the 30–80 keV range, *Engebretson et al.* [2008] further found that waves were associated with precipitation during the recovery phase and conversely the lack of waves during onset and main phase corresponded to an absence of precipitation. This led the authors to suggest the possibility that EMIC waves simply did not occur during the earlier storm phases.

[7] Proton precipitation can be imaged by detecting the Doppler-shifted Lyman-α emission at 121.8 nm emitted by the charge-exchanging precipitating protons. Using this technique, the first global images of the Earth's proton aurora were obtained by the Far Ultraviolet (FUV) Spectrographic Imager (SI) [*Mende et al.*, 2000] onboard the IMAGE satellite [*Burch*, 2000]. Several types of subauroral proton precipitation signatures have been reported and a close association with EMIC waves have been found with each (see review by *Frey* [2007]). These include short duration dayside proton flashes [*Hubert et al.*, 2003; *Fuselier et al.*, 2004] believed to be produced by waves excited by sudden solar wind pressure enhancements, and highly spatially confined proton spots linked to wave generation in corotating outer plasmaspheric structures [*Frey et al.*, 2004; *Yahnin et al.*, 2007].

[8] Another category of subauroral proton precipitation observed by IMAGE FUV is afternoon detached arcs. The term detached refers to the fact that the arcs occur at latitudes equatorward of and separated from the main auroral oval. Thus, at a fixed local time in the ionosphere, there are two bright precipitation regions separated by a few degrees in latitude by a region devoid of precipitation. The detached arcs are relatively large-scale (extending up to 4–5 hours of local time and often >5° in latitude) and long duration (persisting for thirty minutes to several hours) subauroral features. First reported by *Immel et al.* [2002], afternoon detached arcs are comprised of precipitating protons with mean energy in the range of 10's of keV and are devoid of medium energy electron precipitation. Further study found them to be magnetically connected to the overlap region between cold dense plasmaspheric plume material and anisotropic ring current ion distributions in the equatorial plane. This led to the hypothesis that EMIC waves were driving the scattering [*Burch et al.*, 2002; *Spasojević et al.*, 2004, 2005].

[9] Direct evidence of waves in association with the global imaging of afternoon detached arcs has been reported for a number of events both from the ground [*Immel et al.*, 2005] and *in situ* [*Spasojević et al.*, 2005; *Fraser et al.*, 2006]. In addition, using colocated ground-based optical imaging and magnetometer records at a subauroral latitude *Sakaguchi et al.* [2007, 2008] found that as the detached arcs moved equatorward (poleward) the observed wave frequency was higher (lower) consistent with theoretical expectations for EMIC wave generation. Also, the observed frequencies matched the expected frequency for equatorial generation of EMIC waves in the He^+ band. The strong association between the pulsations and the isolated auroras led *Sakaguchi et al.* [2008] to conclude that "[d]ynamics and instabilities in the inner magnetosphere can be monitored as low-latitude emissions away from the ordinary auroral oval."

[10] In the present study, we examine in detail the temporal evolution of afternoon sector proton precipitation. The two detailed cases presented here were part of a 16 event study of afternoon detached arcs by *Spasojević et al.* [2005]. In each event, the detached arcs were shown to map to a globally observed plasmaspheric plume in the presence of hot ion densities and temperature anisotropies favorable for wave growth [e.g., *Spasojević et al.*, 2004] ($n_{ih} > 1$ cm^{-3} and $T_\perp/T_\parallel > 1.25$ as observed at geosynchronous altitude). The analysis presented here suggests that energetic proton precipitation, and corresponding EMIC waves, are a persistent feature within the plume region during geomagnetically disturbed intervals. Precipitation associated the plasmaspheric plume at times appears latitudinally detached from the main proton oval but at other times there is no clear latitudinal separation between the plume-associated precipitation and the main proton oval. Thus, the afternoon sector proton aurora may, at times, have significant contributions from EMIC wave scattering within the plume in the absence of a distinct latitudinally detached subauroral arc. The spatial and temporal evolution of the plume-associated precipitation, including detachment from the main proton oval, is dependent on the driving magnetospheric and solar wind conditions with the cases presented here being 1) a substorm injection and 2) a northward IMF turning.

2. Case 1: Substorm Injection

[11] The first case we examine occurred during a series of geomagnetic storms over the period 7–11 May 2001 (Figure 1). Several intervals of detached subauroral proton precipitation were observed during the storm interval [see *Spasojević et al.*, 2005], but we focus on one specific

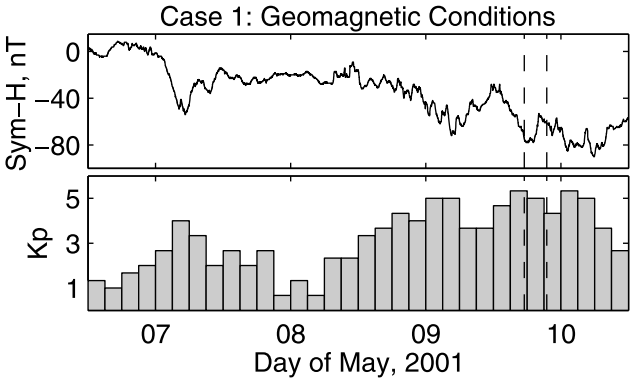

Figure 1. Geomagnetic conditions for Case 1 with (top) the *Sym-H* index, a measure of the strength of the ring current, and (bottom) the K_p index. These data were obtained from the World Data Center for Geomagnetism, Kyoto. The dashed lines indicate the proton precipitation interval examined in detail.

interval late in the day on 9 May 2001 at which time the *Sym-H* index [e.g., *Wanliss and Showalter*, 2006] was near −70 nT. From 18 to 21 UT, the solar wind and IMF were particularly steady (Figure 2) with dynamic pressure and IMF B_z averaging 2.6 nPa and −7.2 nT respectively.

[12] The full series of FUV SI12 proton aurora and Extreme Ultraviolet (EUV) plasmasphere images for this interval can be seen in Animation 1, and snapshots at selected times are shown in Figure 3.[1] Figure 3 (left) is the FUV SI12 observed proton aurora (doppler shifted Lyman-α line at 121.82 nm) mapped to the ionosphere in magnetic apex coordinates [*Richmond*, 1995]. Figure 3 (middle) shows the same FUV image mapped along magnetic field lines to the geocentric solar magnetospheric (GSM) equatorial plane [*Russell*, 1971]. The corners of each SI12 pixel are mapped from the ionosphere at 120 km altitude to the equator using the T96 magnetic field model [*Tsyganenko*, 1995; *Tsyganenko and Stern*, 1996] and the prevailing solar wind conditions. Figure 3 (right) is the closest-in-time EUV image (EUV image cadence is 10 min while FUV SI12 is 2 min) showing the line of sight He^+ column density (30.4 nm). The image has been mapped to the solar magnetic (SM) equatorial plane using the minimum-L technique [*Roelof and Skinner*, 2000] and a dipole field model. The plasmapause location was manually selected [e.g., *Goldstein et al.*, 2003] and is indicated by the magenta line. The points comprising the plasmapause are then remapped using the minimum-L technique and the T96 magnetic field model and translated to the GSM equatorial plane. The plasmapause location is then overlaid on the equatorial FUV image in Figure 3 (middle).

[13] From 18:00 UT (first available image of the orbit) to 19:21 UT (Figure 3a), the proton oval was expanded and relatively stable as a result of the extended period of steady southward IMF. During this period, there is a bright precipitation spot in the afternoon local time sector near 15 MLT that appears as part of the main auroral oval (indicated by the arrow in Figure 3a (left)). This precipitation spot was particularly stable in intensity and latitudinal extent for the 80 min period as can be seen in the keogram of Figure 2c. The keogram displays the average auroral brightness in a half hour wedge of local time (15.25 ± 0.25 h) as a function of magnetic latitude and UT. The EUV image nearest 19:21 UT (Figure 3a, right) shows an eroded plasmasphere from midnight to noon and a sunward extending plasmaspheric plume in the afternoon sector. The plume formed as a result of enhanced convection extending over the past several days [e.g., *Spasojević et al.*, 2003; *Goldstein and Sandel*, 2005]. When mapped to the equatorial plane (Figure 3a, middle), the proton precipitation on the nightside of the Earth appears to map outside the plasmapause to the inner edge of the plasma sheet. On the other hand, the afternoon bright spot near 15 MLT maps within the plasmaspheric plume from 4 to beyond 6 R_E (indicated by the arrow in Figure 3a (middle)).

[14] The mapping of the proton precipitation region to the plasmaspheric plume in the presence of enhanced hot ion densities and temperature anisotropies [see *Spasojević et al.*, 2005], together with the large body of supporting observational and theoretical studies (see Introduction), strongly suggests that the plume-associated proton precipitation is driven by EMIC wave pitch angle scattering. With this assertion, we follow the precipitation pattern in response to a fresh substorm ion injection.

[15] Just after 19:21 UT, an auroral substorm is initiated at about 22.5 MLT. The proton aurora brightens and travels

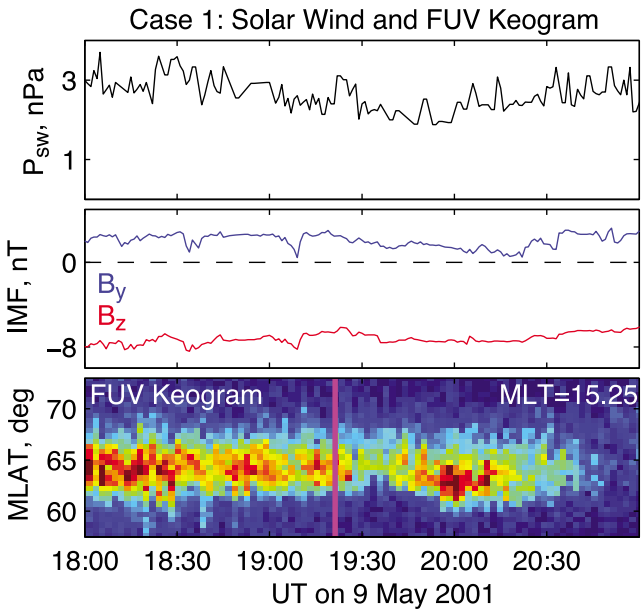

Figure 2. (top and middle) The solar wind dynamic pressure and the IMF B_z (red) and B_y (blue) components. These data were taken from the high resolution OMNIWeb database and represent quantities convected to the Earth's bow shock nose. (bottom) A keogram from the FUV SI12 instrument showing proton auroral brightness as a function of magnetic latitude and UT averaged over a half hour wedge of local time centered at 15.25 MLT. The color scale is the same as that used in Figure 3 with the darkest blue indicating 0.3 kR and the darkest red indicating 2.5 kR. The vertical magenta line indicates the onset time of an auroral substorm in the midnight local time sector.

[1] Animations 1 and 2 are available in the HTML.

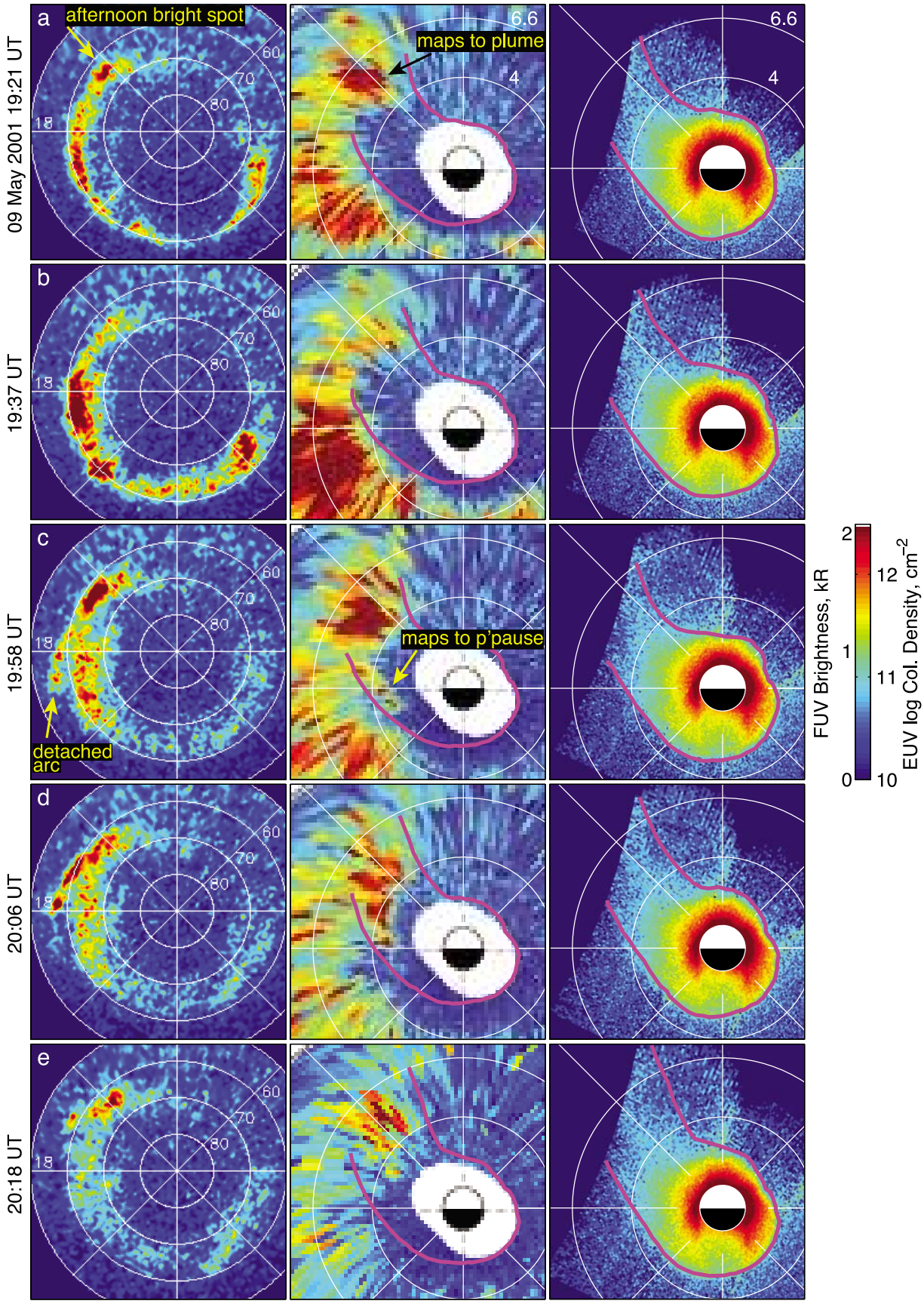
a
afternoon bright spot
6.6
maps to plume
4
6.6
4
09 May 2001 19:21 UT
b
19:37 UT
c
19:58 UT
maps to p'pause
detached arc
d
20:06 UT
e
20:18 UT
60
70
80
18
FUV Brightness, kR
2
1
0
EUV log Col. Density, cm^{-2}
12
11
10

Figure 3

both eastward and westward. At 19:37 UT (Figure 3b), the proton aurora has brightened, expanding both poleward and equatorward, from ~17 to 22 MLT. This region maps outside the duskside plasmapause. The bright spot of precipitation centered at 15 MLT and mapping to the center of the plume persists.

[16] By 19:58 UT (Figure 3c), the proton precipitation in the main oval in the postdusk sector has diminished, but at latitudes below 60°, a latitudinally detached subauroral proton arc is observed extending from ~18 to 19 MLT (indicated by the arrow in Figure 3c (left)). This precipitation region is considered a detached arc since there is a clear region devoid of precipitation between the arc and the main proton oval at higher latitude. The detached arc maps just inside and along the duskside plasmapause boundary at radial distances between ~3 and 5 R_E (indicated by the arrow in Figure 3c (middle)). In addition, the spot of precipitation in the afternoon sector, ~15–16.5 MLT, has significantly brightened and expanded to slightly lower latitudes with the equatorward edge now mapping into the plume at ~4 R_E radial distance.

[17] As previously stated, the plasmasphere-associated precipitation is believed to be driven by EMIC waves. An upper bound estimate of the energy of the protons involved in the resonant interaction can be made using the time delay between the onsets of plasmasphere-associated precipitation at different local times. For example at $L = 4$, there is an ~18 min delay from the initial auroral brightening at 18 MLT to that at 15.5 MLT. Using a dipole magnetic field and a *Maynard and Chen* [1975] normalization of the Volland-Stern [*Volland*, 1973; *Stern*, 1975] electric field with $K_p = 5$, this time delay corresponds to the magnetic and electric drift time of equatorially mirroring protons at 65 keV. This calculation is an upper bound estimate of the energy range since we used the time delay of the initial brightenings, which would correspond to the highest energy protons. Sustained precipitation at a given local time would then be attributed the later arrival of protons of lower energy. A stronger electric field than estimated here would decrease the upper bound energy estimate while a weaker magnetic field (due to dilation of the field by the bulk of the ring current) would increase the estimated energy. Thus, the onset of precipitation along the plasmapause and within the plume is consistent with the expected magnetic and electric drift times of ring current energy protons. Essentially, the substorm resulted in the fresh injection of ions from the plasma sheet into the inner magnetosphere. When these anisotropic ion distributions encountered the cold dense plasmaspheric plasma, the distribution became unstable to EMIC wave growth and subsequently protons were pitch angle scattered into the loss cone. The association of the precipitation region in time with the end of the substorm and in space with the plasmaspheric plume indicates that both the hot ion anisotropy and cold plasma density play important roles in EMIC wave growth.

[18] The observed precipitation pattern continues, and at 20:06 UT (Figure 3d), the plasmasphere-associated precipitation is the brightest auroral feature. By 20:18 UT, the precipitation in the detached arc equatorward of 60° and mapping along the duskside plasmapause has mostly faded, but the plume-associated precipitation near 15 MLT persists. Weaker precipitation within the plume continues until about 20:45 UT as can be seen in the keogram of Figure 2 (bottom).

3. Case 1: Discussion

[19] In Case 1, we followed the evolution of proton precipitation associated with the plasmasphere and believed to be driven by EMIC waves in response to a substorm ion injection. There are two regions of plasmasphere-associated precipitation with different characteristics. The first is the bright precipitation spot centered near 15 MLT. This region of precipitation appeared as part of the main oval (and not as a latitudinally detached arc) but nevertheless clearly maps to the center of the plasmaspheric plume at distances of 4 to 6 R_E. Enhanced precipitation in this region was present for at least 1.5 h prior to the substorm injection. The precipitation spot brightened in response to the substorm injection and persisted for about an hour afterward. The second precipitation region of interest was the detached arc that formed at relatively low latitude and mapped to a narrow region along the duskside plasmapause. This region extended to as low as 3 R_E but was relatively short lived, with the bulk of the precipitation lasting only about 20 min. The narrow radial extent of the precipitation supports theoretical predictions that the steep density gradient at the plasmapause guides waves and leads to enhanced growth rates [*Thorne and Horne*, 1997]. This effect appears to be less important at higher radial distances where the precipitation fills the entire azimuthal extent of the plume. On the other hand, it is known that the plume is permeated by irregular density structure (e.g., *Spasojević et al.* [2003], *Goldstein et al.* [2004], as well as Figure 7) which may act as smaller scale guiding structures.

[20] The shorter duration of the precipitation at smaller radial distances may be understood considering theoretical expectations for EMIC wave growth. For waves a given fraction of the local proton gyrofrequency, the resonant proton energy depends on the factor B^2/n_e (where B is the magnetic field strength and n_e is the cold plasma density) [*Kennel and Petschek*, 1966]. This factor is expected to decrease with increasing radial distance since in the equatorial plane, the strength of the magnetic field decreases as $\sim 1/r^3$ while n_e varies as $\sim 1/r^4$. Thus at lower radial distances, it is only in the immediate aftermath of the substorm that there are a sufficient number of higher energy resonant protons with sufficient anisotropy to produce significant wave growth. In contrast at larger radial distances, resonant energies are lower, and thus there are more protons available

Figure 3. (a–e) A sequence of FUV SI12 proton aurora and EUV plasmasphere images for Case 1, the 09 May 2001 event. For each time, the left panel is the FUV SI12 image mapped to the ionosphere in magnetic APEX coordinates. The middle panel is that same image mapped along geomagnetic field lines, using the T96 magnetic field model and prevailing solar wind conditions, to the GSM equatorial plane. The right panel is the closest-in-time EUV image mapped to the SM equatorial plane using a dipole field model. The location of the plasmapause is indicated by the magenta line, and those points are remapped using a T96 field model and overlaid in the middle panel. Noon is to the top in all images.

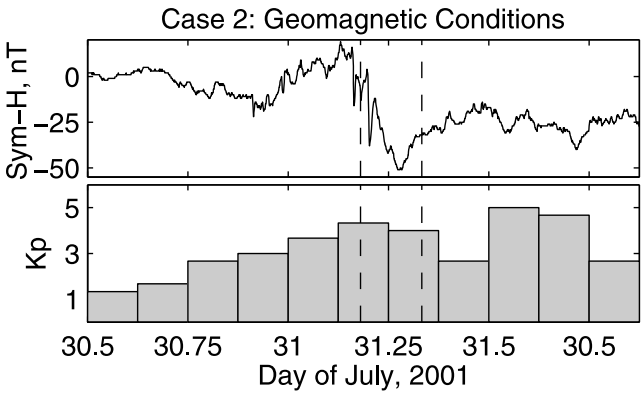

Figure 4. Same as Figure 1 for Case 2.

near resonance. Also, the proton anisotropy may be higher at larger radial distances as a result of drift shell splitting. These factors result in wave generation over an extended period at larger radial distances within the plasmaspheric plume (bright precipitation spot a 15 MLT) while waves in the plasmasphere closer to the Earth are of relatively short duration (detached arc near 18 MLT).

4. Case 2: Northward IMF Turning

[21] The second case we examine occurred during a relatively isolated, minor magnetic storm (minimum *Sym-H* = −51 nT) on 31 July 2001 (Figure 4). In contrast to Case 1, in Case 2 a latitudinally detached arc, associated with the plasmaspheric plume, appears in the aftermath of a northward IMF turning in the absence of an auroral substorm. A large percentage of previously reported afternoon detached arc events have been associated with northward turnings [*Burch et al.*, 2002; *Spasojević et al.*, 2004, 2005]. The solar wind pressure and IMF conditions for the event interval are shown in Figure 5 (top and middle). A clear northward IMF turning can be seen at 06:11 UT.

[22] Figure 5 (bottom) shows a keogram derived from the FUV SI12 imager centered at 14.75 MLT. One noticeable feature of the keogram is an ∼12 min oscillation wherein aurora features appear to move by ∼1° in latitude. During the summer months, the IMAGE spacecraft star tracker has interference from stray sunlight. The less accurate star sensor must be used, resulting in an apparent wobble in the image. Despite this wobble, the large scale features of the proton aurora are still clearly visible.

[23] The global evolution of the proton auroral during the entire event period can be seen in Animation 2 and selected snapshots are shown in Figure 6. In the first image of the interval at 05:58 UT (Figure 6a), the entire aurora oval is bright and expanded to lower latitudes. Unfortunately, as a result of the viewing geometry, the entire plasmasphere is not within the EUV field of view. However, a well-defined plasmapause can be seen from dusk counterclockwise around to noon, and a region of cold plasma extends outside of the field of view in the afternoon sector. This apparent plume feature is supported by measurements of enhanced cold plasma at geosynchronous orbit (6.6 R_E) by the MPA instruments [*Bame et al.*, 1993] on the 1991-080 and 1994-084 spacecraft. As shown in Figure 7, both geosynchronous spacecraft observed enhanced cold plasma in the afternoon sector at ∼14−19 MLT. At the time of the northward IMF turning, 1994-084 observed plume material with peak values exceeding 50 cm^{-3}.

[24] When mapped to the equatorial plane, the proton precipitation region at 05:58 UT (Figure 6a) is outside the plasmapause boundary from ∼21 MLT to 06 MLT, but in the dusk sector (∼18 to 21 MLT) there is precipitation that maps both inside and outside the boundary. The equatorward edge of the proton precipitation maps to the equatorial plane inside the plasmapause at radial distances as low as 3 R_E in the postdusk sector. At earlier local times, ∼15 MLT, the proton precipitation region extends from ∼4 to 6.6 R_E within region of enhanced cold plasma density.

[25] The bright afternoon sector auroral precipitation began around 05:45 UT as seen in the keogram of Figure 5 centered at 14.75 MLT. The IMF had been strongly southward for the previous hour and thus enhanced convection had resulting in an intensification of the ring current (interval approaching the minimum *Sym-H* in Figure 4). Thus, as in Case 1, we assert that the proton precipitation that maps to the region inside the plasmasphere and plume region as observed by EUV and *in situ* by the MPA instruments is the result of EMIC wave-induced scattering.

[26] At 06:27 UT, a slight splitting of the duskside oval can be seen (indicated by the arrow in Figure 6b (left)). The split maps to the location of the plasmapause boundary (indicated by the arrow in Figure 6b (middle)). The main proton oval begins to retreat poleward and reduce in brightness in the next several snapshots (Figures 6c−6e). However, the region of precipitation at lower latitudes that maps inside the plasmapause in the dusk and afternoon sectors persists. This can also be clearly seen in the keogram of Figure 5 where, in the aftermath of the northward IMF turning

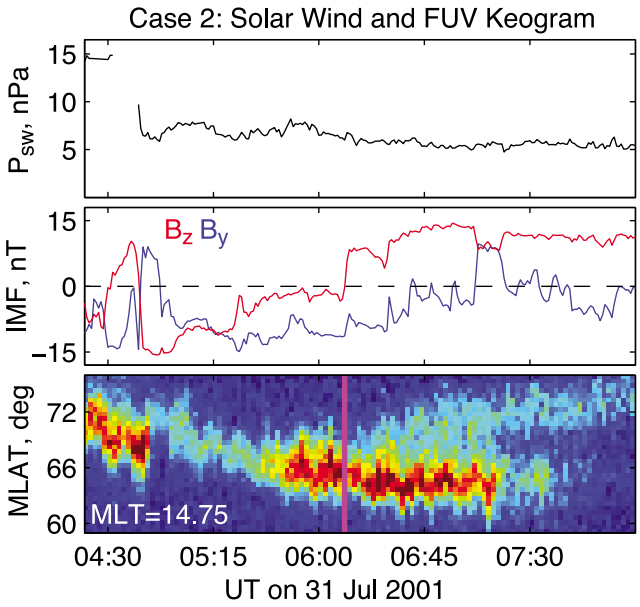

Figure 5. Same as Figure 2 for Case 2. There is a 10 min gap in the dynamic pressure data starting at 4:33 UT. The keogram is centered at 14.75 MLT, and the magenta line indicates the time of the northward IMF turning. The color scale is the same as that used in Figure 3 with the darkest blue indicating 0.3 kR and the darkest red indicating 4 kR.

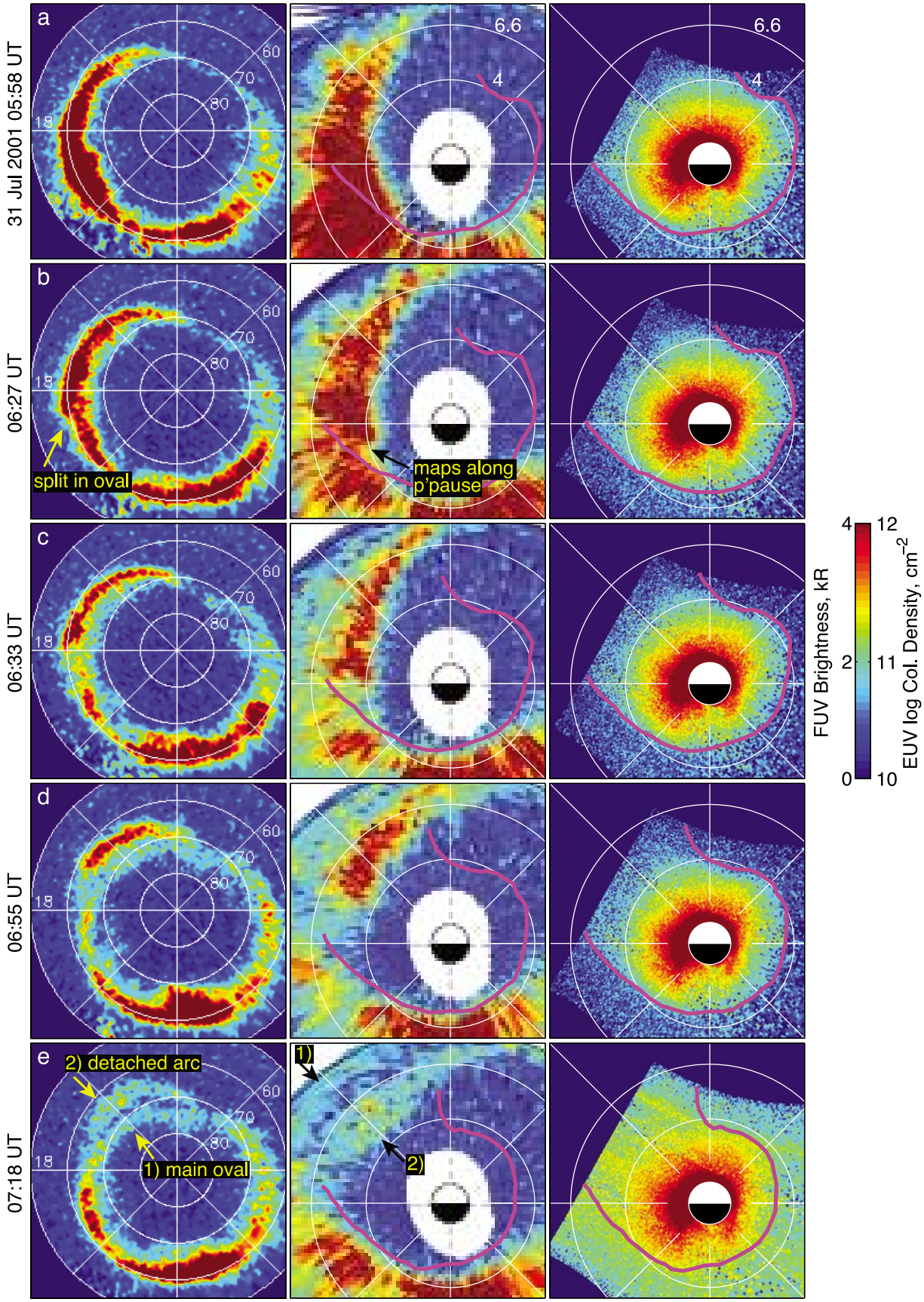

Figure 6. (a–e) Same as Figure 3 for Case 2. In Figure 6e, the EUV image is contaminated by high background, and column density values are invalid.

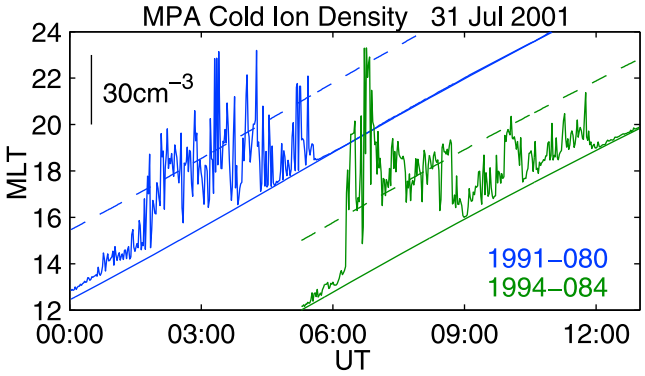

Figure 7. The location of geosynchronous spacecraft 1991-080 and 1994-084 as a function of MLT and UT (solid diagonal line). The measured cold ion density is indicated by the height of the colored line above the orbit track with the dashed colored line indicating a density of 30 cm^{-3}.

(magenta line), the bright plasmasphere-associated precipitation remains near 64° latitude while a weaker arc peels off poleward. The poleward feature is the main auroral oval and is presumed to be associated with the plasma sheet and/or dayside boundary layer region.

[27] In the images from ~06:30 to 07:00 UT (Figures 6c and 6d and Animation 2), the eastern edge of plume-associated precipitation region gradually retreats to earlier local times. This is consistent with the fact that convection and thus the supply of anisotropy protons from the plasma sheet has ceased. By 07:18 UT in the afternoon sector (Figure 6e), it can be clearly seen the plasmasphere-associated precipitation is latitudinally detached from the main proton oval (indicated by the arrows in Figure 6e (left and middle). The plume-associated precipitation continues to fade with time, but weaker precipitation persists for another half hour.

5. Case 2: Discussion

[28] An interval of strongly southward IMF resulted in the expansion of the entire auroral oval to lower latitudes. At the same time, enhanced convection acted to build up the ring current in the inner magnetosphere and the transport plasmaspheric material sunward. The proton oval was bright in the afternoon sector, and we contend that precipitating protons in that region originated from two distinct sources. The poleward edge of the oval likely consists of protons scattered in the plasma sheet and/or the dayside boundary layers whereas the equatorward edge, and possibly the bulk of the precipitation, results from EMIC wave scattering in the ring current/plasmasphere overlap region. These two sources of precipitating protons merge into one in the auroral images as a result of the convergence of field lines into the ionosphere, multiple scattering of protons in the atmosphere and the point spread function of the instrument. It is possible that the two regions could be distinctly resolved with ground-based optical instrumentation [i.e., *Sakaguchi et al.*, 2008].

[29] When the IMF turned northward, the main oval retreated poleward and a clear gap is seen between the intense EMIC scattered protons at lower latitude from within the plasmasphere and the weaker boundary layer precipitation at higher latitude. We believe that the wave-induced precipitation within the plasmasphere persisted for a total of nearly 2.5 h, but the region only appeared as a latitudinally detached arc in the aftermath of the northward IMF turning. In addition, after the northward turning, convection ceased. Thus, no new ions were convected in from the plasma sheet, the existing ring current distributions stabilized, and the plasmasphere-associated precipitation gradually faded.

6. Conclusions

[30] Our analysis here suggests that energetic proton precipitation may be a persistent feature within the afternoon sector plasmasphere and plasmaspheric plume during disturbed intervals. Past work on plume-associated precipitation regions using global proton aurora images [*Burch et al.*, 2002; *Spasojević et al.*, 2004, 2005] has focused on intervals when the precipitation regions appear as latitudinally detached from the main protons oval. Our findings here show that plume-associated precipitation at times appears detached from the main proton oval but at other times there is no clear latitudinal separation. The spatial and temporal evolution of the plume-associated precipitation, including possible detachment from the main oval, is dependent on the specific magnetospheric and solar wind driving conditions with the cases presented here being 1) a substorm injection and 2) a northward IMF turning. Thus, the equatorward portion of the afternoon sector proton auroral oval may have significant contributions from EMIC wave scattering occurring within the plasmasphere and plasmaspheric plume in the absence of a distinct detached arc.

[31] We find that the lowest latitude precipitation, that which maps inside L = 4, is confined to the region of the steep density gradient along the plasmapause boundary. This plasmapause-associated precipitation persists only during active driving, such as a substorm injection or strong convection. Our finding is consistent with theoretical expectations that hot ion density, hot ion anisotropy and cold plasma density are all important parameters in EMIC wave growth. Precipitation mapping to the plasmaspheric plume at higher L (>4.5) can persist for several hours in the cases examined and perhaps longer in large storm events. Wave growth in the higher L region is favored since resonant proton energies are lower and temperature anisotropies are expected to be higher as a result of drift shell splitting. In addition, density irregularities are ubiquitous in the plume (particularly as measured at geosynchronous altitude), and these structures may act to guide waves along the field line further contributing to enhanced wave growth rates in this region.

[32] Whether the plume-associated precipitation regions appear latitudinally detached from the main proton oval depends, in part, on the size and shape of the main oval. For example, during intervals of strongly southward IMF, the entire oval expands to lower latitude. At these times, plume-associated precipitation driven by EMIC waves and precipitation from the plasma sheet and/or dayside boundary layer region appear within the ionosphere as one contiguous precipitation band. This is the result of the convergence of field lines in the ionosphere as well as the resolution and

response of the global imager. A northward turning of IMF causes the boundary layer precipitation to move to higher latitudes, creating a separation between the higher latitude main oval and the lower latitude plume-associated precipitation. *Burch et al.* [2002] also reported a case when a detached arc appeared as a result of a westward to eastward turning of the IMF (B_y rotation from negative to positive), which resulted in a poleward contraction of the main oval specifically in the afternoon sector.

[33] The data presented here in conjunction with past observational and theoretical work strongly supports the hypothesis that the observed precipitation associated with the plasmapause and plume is the result of EMIC wave scattering. Further, the location and duration of plasmasphere-associated precipitation is a positive proxy indicator for the distribution of EMIC waves in the inner magnetosphere. By positive proxy indicator, we mean that the location of plasmasphere-associated proton precipitation can be used as an indirect measure of the location of EMIC waves. A full proxy relationship cannot be claimed since the absence of detectable precipitation does not necessarily indicate a lack of waves. From a theoretical standpoint, if EMIC waves grow to saturation, then they must reduce the free energy of the plasma. That is, they must pitch angle scatter the energetic protons toward the loss cone. There may, however, be times when the waves are present but scattering into the loss cone may be weak and undetectable by the imager. Nevertheless, the positive proxy indicator may be of use for studies of the inner magnetosphere. For example, knowledge of the EMIC wave distribution has potential application not just for studies of ring current proton losses but also for evaluating EMIC contributions to relativistic electron precipitation.

[34] **Acknowledgments.** We are grateful to the Kyoto World Data Center for providing the geomagnetic indices, the OMNIWEB database for providing solar wind data, and M. F. Thomsen for providing the LANL MPA data. This research was supported by NASA grant NNX07AG52G.

[35] Zuyin Pu thanks the reviewers for their assistance in evaluating this manuscript.

References

Anderson, B. J., and D. C. Hamilton (1993), Electromagnetic ion cyclotron waves stimulated by modest magnetospheric compressions, *J. Geophys. Res.*, *98*, 11,369–11,382.

Anderson, B. J., R. E. Erlandson, and L. J. Zanetti (1992a), A statistical study of Pc 1–2 magnetic pulsations in the equatorial magnetosphere: 1. Equatorial occurrence distributions, *J. Geophys. Res.*, *97*, 3075–3088.

Anderson, B. J., R. E. Erlandson, and L. J. Zanetti (1992b), A statistical study of Pc 1–2 magnetic pulsations in the equatorial magnetosphere: 2. Wave properties, *J. Geophys. Res.*, *97*, 3089–3101.

Bame, S. J., et al. (1993), Magnetospheric plasma analyzer for spacecraft with constrained resources, *Rev. Sci. Instrum.*, *64*, 1026–1033.

Bortnik, J., R. M. Thorne, T. P. O'Brien, J. C. Green, R. J. Strangeway, Y. Y. Shprits, and D. N. Baker (2006), Observation of two distinct, rapid loss mechanisms during the 20 November 2003 radiation belt dropout event, *J. Geophys. Res.*, *111*, A12216, doi:10.1029/2006JA011802.

Bräysy, T., K. Mursula, and G. Marklund (1998), Ion cyclotron waves during a great magnetic storm observed by Freja double-probe electric field instrument, *J. Geophys. Res.*, *103*, 4145–4156.

Burch, J. L. (2000), IMAGE mission overview, *Space Sci. Rev.*, *91*, 1–14.

Burch, J. L., W. S. Lewis, T. J. Immel, P. C. Anderson, H. U. Frey, S. A. Fuselier, J.-C. Gérard, S. B. Mende, D. G. Mitchell, and M. F. Tomsen (2002), Interplanetary magnetic field control of afternoon-sector detached proton auroral arcs, *J. Geophys. Res.*, *107*(A9), 1251, doi:10.1029/2001JA007554.

Cornwall, J. M., F. V. Coroniti, and R. M. Thorne (1971), Unified theory of SAR arc formation at the plasmapause, *J. Geophys. Res.*, *76*, 4428–4445.

Engebretson, M. J., et al. (2008), Pc1–Pc2 waves and energetic particle precipitation during and after magnetic storms: Superposed epoch analysis and case studies, *J. Geophys. Res.*, *113*, A01211, doi:10.1029/2007JA012362.

Erlandson, R. E., and A. J. Ukhorskiy (2001), Observations of electromagnetic ion cyclotron waves during geomagnetic storms: Wave occurrence and pitch angle scattering, *J. Geophys. Res.*, *106*, 3883–3896.

Fraser, B. J., and T. S. Nguyen (2001), Is the plasmapause a preferred source region of electromagnetic ion cyclotron waves in the magnetosphere?, *J. Atmos. Sol. Terr. Phys.*, *63*, 1225–1247.

Fraser, B. J., J. C. Samson, Y. D. Hu, R. L. McPherron, and C. T. Russell (1992), Electromagnetic ion cyclotron waves observed near the oxygen cyclotron frequency by ISEE 1 and 2, *J. Geophys. Res.*, *97*, 3063–3074.

Fraser, B. J., H. J. Singer, W. J. Hughes, J. R. Wygant, R. R. Anderson, and Y. D. Hu (1996), CRRES Poynting vector observations of electromagnetic ion cyclotron waves near the plasmapause, *J. Geophys. Res.*, *101*, 15,331–15,343.

Fraser, B. J., T. M. Loto'aniu, and H. J. Singer (2006), Electromagnetic ion cyclotron waves in the magnetosphere, in *Magnetospheric ULF Waves: Synthesis and New Directions*, *Geophys. Monogr. Ser.*, vol. 169, edited by K. Takahashi et al., pp. 195–212, AGU, Washington, D. C.

Frey, H. U. (2007), Localized aurora beyond the auroral oval, *Rev. Geophys.*, *45*, RG1003, doi:10.1029/2005RG000174.

Frey, H. U., G. Haerendel, S. B. Mende, W. T. Forrester, T. J. Immel, and N. Østgaard (2004), Subauroral morning proton spots (SAMPS) as a result of plasmapause-ring-current interaction, *J. Geophys. Res.*, *109*, A10305, doi:10.1029/2004JA010516.

Fuselier, S. A., S. P. Gary, M. F. Thomsen, E. S. Claflin, B. Hubert, B. R. Sandel, and T. Immel (2004), Generation of transient dayside subauroral proton precipitation, *J. Geophys. Res.*, *109*, A12227, doi:10.1029/2004JA010393.

Goldstein, J., and B. R. Sandel (2005), The global pattern of evolution of plasmaspheric drainage plumes, in *Inner Magnetosphere Interactions: New Perspectives From Imaging*, *Geophys. Monogr. Ser.*, vol. 159, edited by J. Burch, M. Schulz, and H. Spence, pp. 1–22, AGU, Washington, D. C.

Goldstein, J., M. Spasojević, P. H. Reiff, B. R. Sandel, W. T. Forrester, D. L. Gallagher, and B. W. Reinisch (2003), Identifying the plasmapause in IMAGE EUV data using IMAGE RPI in situ steep density gradients, *J. Geophys. Res.*, *108*(A4), 1147, doi:10.1029/2002JA009475.

Goldstein, J., B. R. Sandel, M. F. Thomsen, M. Spasojević, and P. H. Reiff (2004), Simultaneous remote sensing and in situ observations of plasmaspheric drainage plumes, *J. Geophys. Res.*, *109*, A03202, doi:10.1029/2003JA010281.

Gurgiolo, C., B. R. Sandel, J. D. Perez, D. G. Mitchell, C. J. Pollock, and B. A. Larsen (2005), Overlap of the plasmasphere and ring current: Relation to subauroral ionospheric heating, *J. Geophys. Res.*, *110*, A12217, doi:10.1029/2004JA010986.

Horne, R. B., and R. M. Thorne (1997), Wave heating of He^+ by electromagnetic ion cyclotron waves in the magnetosphere: Heating near the H^+-He^+ bi-ion resonance frequency, *J. Geophys. Res.*, *102*, 11,457–11,472.

Hubert, B., J.-C. Gérard, S. A. Fuselier, and S. B. Mende (2003), Observation of dayside subauroral proton flashes with IMAGE-FUV, paper 2267 presented at EGS-AGU-EUG Joint Assembly, Nice, France, 6–11 April.

Immel, T. J., S. B. Mende, H. U. Frey, L. M. Peticolas, C. W. Carlson, J.-C. Gérard, B. Hubert, S. A. Fuselier, and J. L. Burch (2002), Precipitation of auroral protons in detached arcs, *Geophys. Res. Lett.*, *29*(11), 1519, doi:10.1029/2001GL013847.

Immel, T. J., S. B. Mende, H. U. Frey, J. Patel, J. W. Bonnell, M. J. Engebretson, and S. A. Fuselier (2005), ULF waves associated with enhanced subauroral proton precipitation, in *Inner Magnetosphere Interactions: New Perspectives From Imaging*, *Geophys. Monogr. Ser.*, vol. 159, edited by J. Burch, M. Schulz, and H. Spence, pp. 71–84, AGU, Washington, D. C.

Jordanova, V. K., M. Spasojevic, and M. F. Thomsen (2007), Modeling the electromagnetic ion cyclotron wave-induced formation of detached subauroral proton arcs, *J. Geophys. Res.*, *112*, A08209, doi:10.1029/2006JA012215.

Jordanova, V. K., J. Albert, and Y. Miyoshi (2008), Relativistic electron precipitation by EMIC waves from self-consistent global simulations, *J. Geophys. Res.*, *113*, A00A10, doi:10.1029/2008JA013239.

Kangas, J., A. Guglielmi, and O. Pokhotelov (1998), Morphology and physics of short-period magnetic pulsations, *Space Sci. Rev.*, *83*, 435–512.

Kennel, C. F., and H. E. Petschek (1966), Limit on stably trapped particle fluxes, *J. Geophys. Res.*, *71*, 1–28.

Khazanov, G. V., K. V. Gamayunov, D. L. Gallagher, J. U. Kozyra, and M. W. Liemohn (2007), Self-consistent model of magnetospheric ring current and propagating electromagnetic ion cyclotron waves: 2. Wave-induced ring current precipitation and thermal electron heating, *J. Geophys. Res.*, *112*, A04209, doi:10.1029/2006JA012033.

Lyons, L. R., and R. M. Thorne (1972), Parasitic pitch angle diffusion of radiation belt particles by ion cyclotron waves, *J. Geophys. Res.*, *77*, 5608–5616.

Maynard, N. C., and A. J. Chen (1975), Isolated cold plasma regions: Observations and their relation to possible production mechanisms, *J. Geophys. Res.*, *80*, 1009–1013.

Mende, S. B., et al. (2000), Far ultraviolet imaging from the IMAGE spacecraft. 3. Spectral imaging of Lyman-α and OI 135.6 nm, *Space Sci. Rev.*, *91*, 287–318.

Meredith, N. P., R. M. Thorne, R. B. Horne, D. Summers, B. J. Fraser, and R. R. Anderson (2003), Statistical analysis of relativistic electron energies for cyclotron resonance with EMIC waves observed on CRRES, *J. Geophys. Res.*, *108*(A6), 1250, doi:10.1029/2002JA009700.

Millan, R. M., R. P. Lin, D. M. Smith, K. R. Lorentzen, and M. P. McCarthy (2002), X-ray observations of MeV electron precipitation with a balloon-borne germanium spectrometer, *Geophys. Res. Lett.*, *29*(24), 2194, doi:10.1029/2002GL015922.

Richmond, A. D. (1995), Ionospheric electrodynamics using magnetic apex coordinates, *J. Geomagn. Geoelectr.*, *47*, 191–212.

Roelof, E. C., and A. J. Skinner (2000), Extraction of ion distributions from magnetospheric ENA and EUV images, *Space Sci. Rev.*, *91*, 437–459.

Russell, C. T. (1971), Geophysical coordinate transformations, *Cosmic Electrodyn*, *2*, 184–196.

Sakaguchi, K., K. Shiokawa, A. Ieda, Y. Miyoshi, Y. Otsuka, T. Ogawa, M. Connors, E. F. Donovan, and F. J. Rich (2007), Simultaneous ground and satellite observations of an isolated proton arc at subauroral latitudes, *J. Geophys. Res.*, *112*, A04202, doi:10.1029/2006JA012135.

Sakaguchi, K., K. Shiokawa, Y. Miyoshi, Y. Otsuka, T. Ogawa, K. Asamura, and M. Connors (2008), Simultaneous appearance of isolated auroral arcs and Pc 1 geomagnetic pulsations at subauroral latitudes, *J. Geophys. Res.*, *113*, A05201, doi:10.1029/2007JA012888.

Sergeev, V. A., G. R. Bikkuzina, and P. T. Newell (1997), Dayside isotropic precipitation of energetic protons, *Ann. Geophys.*, *15*, 1233–1245.

Søraas, F., J. Å. Lundblad, N. F. Maltseva, V. Troitskaya, and V. Selivanov (1980), A comparison between simultaneous I.P.D.P. groundbased observations and observations of energetic protons obtained by satellites, *Planet. Space Sci.*, *28*, 387–405.

Spasojević, M., J. Goldstein, D. L. Carpenter, U. S. Inan, B. R. Sandel, M. B. Moldwin, and B. W. Reinisch (2003), Global response of the plasmasphere to a geomagnetic disturbance, *J. Geophys. Res.*, *108*(A9), 1340, doi:10.1029/2003JA009987.

Spasojević, M., H. U. Frey, M. F. Thomsen, S. A. Fuselier, S. P. Gary, B. R. Sandel, and U. S. Inan (2004), The link between a detached subauroral proton arc and a plasmaspheric plume, *Geophys. Res. Lett.*, *31*, L04803, doi:10.1029/2003GL018389.

Spasojević, M., M. F. Thomsen, P. J. Chi, and B. R. Sandel (2005), Afternoon subauroral proton precipitation resulting from ring current–plasmasphere interaction, in *Inner Magnetosphere Interactions: New Perspectives From Imaging*, *Geophys. Monogr. Ser.*, vol. 159, edited by J. Burch, M. Schulz, and H. Spence, pp. 85–99, AGU, Washington, D. C.

Stern, D. P. (1975), The motion of a proton in the equatorial magnetosphere, *J. Geophys. Res.*, *80*, 595–599.

Thorne, R. M., and R. B. Horne (1992), The contribution of ion-cyclotron waves to electron heating and SAR-arc excitation near the storm-time plasmapause, *Geophys. Res. Lett.*, *19*, 417–420.

Thorne, R. M., and R. B. Horne (1993), Cyclotron absorption of ion cyclotron waves at the bi-ion frequency, *Geophys. Res. Lett.*, *20*, 317–320.

Thorne, R. M., and R. B. Horne (1994), Energy transfer between energetic ring current H^+ and O^+ by electromagnetic ion cyclotron waves, *J. Geophys. Res.*, *99*, 17,275–17,282.

Thorne, R. M., and R. B. Horne (1997), Modulation of electromagnetic ion cyclotron instability due to interaction with ring current O^+ during magnetic storms, *J. Geophys. Res.*, *102*, 14,155–14,163.

Thorne, R. M., and C. F. Kennel (1971), Relativistic electron precipitation during magnetic storm main phase, *J. Geophys. Res.*, *76*, 4446–4453.

Tsyganenko, N. A. (1995), Modeling the Earth's magnetospheric magnetic field confined within a realistic magnetopause, *J. Geophys. Res.*, *100*, 5599–5612.

Tsyganenko, N. A., and D. P. Stern (1996), Modeling the global magnetic field of the large-scale Birkeland current systems, *J. Geophys. Res.*, *101*, 27,187–27,198.

Volland, H. (1973), A semiempirical model of large-scale magnetospheric electric fields, *J. Geophys. Res.*, *78*, 171–180.

Wanliss, J. A., and K. M. Showalter (2006), High-resolution global storm index: *Dst* versus SYM-H, *J. Geophys. Res.*, *111*, A02202, doi:10.1029/2005JA011034.

Yahnin, A. G., T. A. Yahnina, and H. U. Frey (2007), Subauroral proton spots visualize the Pc1 source, *J. Geophys. Res.*, *112*, A10223, doi:10.1029/2007JA012501.

Yahnina, T. A., A. G. Yahnin, J. Kangas, and J. Manninen (2000), Proton precipitation related to Pc1 pulsations, *Geophys. Res. Lett.*, *27*, 3575–3578.

Yahnina, T. A., A. G. Yahnin, J. Kangas, and J. Manninen (2002), Localized enhancements of energetic proton fluxes at low altitudes in the subauroral region and their relation to the Pc1 pulsations, *Cosmic Res.*, *40*, 213–223.

Yahnina, T. A., et al. (2003), Energetic particle counterparts for geomagnetic pulsations of Pc1 and IPDP types, *Ann. Geophys.*, *21*, 2281–2292.

S. A. Fuselier and M. Spasojevic, Lockheed Martin Advanced Technology Center, Palo Alto, CA 94304-1191, USA. (mariaspasojevic@stanford.edu)